NAVAL POSTGRADUATE SCHOOL

MONTEREY, CALIFORNIA

THESIS

ANALYSIS OF RADIATION EFFECTS ON GALLIUM NITRIDE ZIRCONIUM OXIDE METAL OXIDE SEMICONDUCTOR CAPACITORS

by

Connor M. Reasoner Blasch

September 2020

Thesis Advisor:	Todd R. Weatherford
Co-Advisor:	Travis Anderson, U.S. Naval Research Laboratory
Second Reader:	Matthew A. Porter

THIS PAGE INTENTIONALLY LEFT BLANK

REPORT DOCUMENTATION PAGE			*Form Approved OMB No. 0704-0188*

1. AGENCY USE ONLY *(Leave blank)*	**2. REPORT DATE** September 2020	**3. REPORT TYPE AND DATES COVERED** Master's thesis

4. TITLE AND SUBTITLE ANALYSIS OF RADIATION EFFECTS ON GALLIUM NITRIDE ZIRCONIUM OXIDE METAL OXIDE SEMICONDUCTOR CAPACITORS	**5. FUNDING NUMBERS** REN10
6. AUTHOR(S) Connor M. Reasoner Blasch	
7. PERFORMING ORGANIZATION NAME(S) AND ADDRESS(ES) Naval Postgraduate School Monterey, CA 93943-5000	**8. PERFORMING ORGANIZATION REPORT NUMBER**
9. SPONSORING / MONITORING AGENCY NAME(S) AND ADDRESS(ES) DTRA, Fort Belvoir, VA	**10. SPONSORING / MONITORING AGENCY REPORT NUMBER**

11. SUPPLEMENTARY NOTES The views expressed in this thesis are those of the author and do not reflect the official policy or position of the Department of Defense or the U.S. Government.

12a. DISTRIBUTION / AVAILABILITY STATEMENT Approved for public release. Distribution is unlimited.	**12b. DISTRIBUTION CODE** A

13. ABSTRACT (maximum 200 words)

In this work, Gallium Nitride Zirconium oxide metal oxide semiconductor capacitors were exposed to a 40MeV proton beam and a 15MeV Argon heavy ion beam of radiation. Characterization of each device was done using an Agilent B1500A, switch matrix, custom-printed circuit board while using a LabVIEW program to analyze the Capacitance-Voltage (C-V), Capacitance-Frequency (C-F), and Current-Voltage (I-V) measurement prior to and post exposure. Each reticle's C-V measurement and its hysteresis was then compared pre- and post-exposure for effects. Testing concluded with a time-dependent dielectric breakdown analysis. Results show that radiation exposure shifts the capacitance of the device and affects the hysteresis in its C-V measurement. Initial time-dependent dielectric breakdown data shows that devices exposed to certain fluences of radiation will extend the time it takes before oxide breakdown.

14. SUBJECT TERMS Gallium Nitride, Zirconium Oxide, radiation effects, capacitors	**15. NUMBER OF PAGES** 51
	16. PRICE CODE

17. SECURITY CLASSIFICATION OF REPORT	**18. SECURITY CLASSIFICATION OF THIS PAGE**	**19. SECURITY CLASSIFICATION OF ABSTRACT**	**20. LIMITATION OF ABSTRACT**
Unclassified	Unclassified	Unclassified	UU

NSN 7540-01-280-5500 Standard Form 298 (Rev. 2-89) Prescribed by ANSI Std. 239-18

THIS PAGE INTENTIONALLY LEFT BLANK

Approved for public release. Distribution is unlimited.

ANALYSIS OF RADIATION EFFECTS ON GALLIUM NITRIDE ZIRCONIUM OXIDE METAL OXIDE SEMICONDUCTOR CAPACITORS

Connor M. Reasoner Blasch
Lieutenant, United States Navy
BSEE, The Citadel, 2014

Submitted in partial fulfillment of the
requirements for the degree of

MASTER OF SCIENCE IN ELECTRICAL ENGINEERING

from the

NAVAL POSTGRADUATE SCHOOL
September 2020

Approved by: Todd R. Weatherford
Advisor

Travis Anderson
Co-Advisor

Matthew A. Porter
Second Reader

Douglas J. Fouts
Chair, Department of Electrical and Computer Engineering

THIS PAGE INTENTIONALLY LEFT BLANK

ABSTRACT

In this work, Gallium Nitride Zirconium oxide metal oxide semiconductor capacitors were exposed to a 40MeV proton beam and a 15MeV Argon heavy ion beam of radiation. Characterization of each device was done using an Agilent B1500A, switch matrix, custom-printed circuit board while using a LabVIEW program to analyze the Capacitance-Voltage (C-V), Capacitance-Frequency (C-F), and Current-Voltage (I-V) measurement prior to and post exposure. Each reticle's C-V measurement and its hysteresis was then compared pre- and post-exposure for effects. Testing concluded with a time-dependent dielectric breakdown analysis. Results show that radiation exposure shifts the capacitance of the device and affects the hysteresis in its C-V measurement. Initial time-dependent dielectric breakdown data shows that devices exposed to certain fluences of radiation will extend the time it takes before oxide breakdown.

THIS PAGE INTENTIONALLY LEFT BLANK

Table of Contents

1 Introduction **1**
1.1 Research Objective 1
1.2 Related Work 2
1.3 Thesis Organization 2

2 Background **5**
2.1 Fundamentals of MOS Capacitors. 5
2.2 Properties of GaN MOS Capacitors 7
2.3 Radiation Effects 9

3 Experiment **11**
3.1 Composition of Devices and Testing Layout. 11
3.2 Initial Characterization of Devices 12
3.3 Radiation Effects Testing 14
3.4 Post-Irradiation Characterization and Testing 16
3.5 Time-Dependent Dielectric Breakdown Testing 16

4 Results of Analysis **17**
4.1 Analysis of Devices Radiated by Protons 17
4.2 Analysis of Parts Radiated by Protons with Positive Bias Voltage 19
4.3 Analysis of Parts Radiated by Argon Heavy Ions with Positive Bias Voltage . 20
4.4 Analysis of Time-Dependent Dielectric Breakdown Testing 22
4.5 Discussion of Results. 23

5 Conclusions **27**
5.1 Future Work Considerations 27

Appendix: Additional Figure and Tables **29**

A.1 Test Layout for QFN chip 29
A.2 Radiation Test Plan 29

List of References **31**

Initial Distribution List **33**

List of Figures

Figure 2.1 Perspective and cross-section view of a MOS capacitor. Source: [8]. 5

Figure 2.2 (a) High-frequency C-V curve (on p-semiconductor), shifted along the voltage axis due to positive oxide charges; (b) Band diagram at flat band, original; (c) With positive oxide charges; and (d) new flat-band bias. Source: [10]. 7

Figure 2.3 Shown is the comparision of the theoretical limiting Figure of Merit of PMAD technology vs. breakdown voltage. Source: [13]. 9

Figure 3.1 Cross-section of GaN MOSCAPs used for radiation exposure testing. 11

Figure 3.2 Top view of Printed Circuit Board (PCB) utilized for this work. . 12

Figure 3.3 PCB used to characterize devices in actual test bed with printed holder. 13

Figure 3.4 Test board used for bias testing at Cyclotron Institute at Texas A&M. 15

Figure 4.1 a) - c) shows reticle 8 devices pre- and post-proton dose with short radiation C-V measurements with area of hysteresis. 18

Figure 4.2 a) and b) shows reticle 6 devices pre- and post-proton dose with short radiation C-V measurements with area of hysteresis. 19

Figure 4.3 a) - c) shows reticle 3 devices pre- and post-proton with positive bias radiation C-V measurements with area of hysteresis. 20

Figure 4.4 a) and b) shows reticle 12 devices pre- and post-heavy ion with positive bias radiation C-V measurements with area of hysteresis. 21

Figure 4.5 a) - c) shows reticle 5 devices pre- and post-heavy ion with positive bias radiation C-V measurements with area of hysteresis. 22

Figure 4.6 Scatter plot showing each exposure type and their average time of oxide breakdown vs. stress voltage 23

Figure 4.7 a) shows an example of the band diagram of the devices tested at zero bias. Figure b) shows what the band diagram of the devices at bias after heavy ion with positive stress bias radiation exposure. Figure c) shows what the band diagram of the devices after proton with positive stress bias radiation exposure. 24

Figure A.1 Bonding diagram of reticles in QFN packaging 29

List of Tables

Table 3.1 Tables showing each measurement used during characterization. . 14

Table A.1 Table showing each device tested during dose radiation with device shorted for 40MeV proton beam. 29

Table A.2 Table showing each device tested during proton with positive bias testing for 40MeV proton beam. 30

Table A.3 Table showing each device tested during heavy ion with positive bias testing for 15MeV argon beam. 30

THIS PAGE INTENTIONALLY LEFT BLANK

List of Acronyms and Abbreviations

ALD	Atomic Layer Deposition
DoD	Department of Defense
GaAs	Gallium Arsenide
GaN	Gallium Nitride
HEMTs	high electron mobility transistors
MOS	Metal Oxide Semiconductor
MOSFET	Metal Oxide Semiconductor Field Effect Transistor
NIEL	non-ionizing energy loss
NPS	Naval Postgraduate School
NRL	U.S. Naval Research Laboratory
PCB	Printed Circuit Board
SiC	Silicon Carbide
TDDB	time-dependent dielectric breakdown
U.S.	United States
USN	U.S. Navy

THIS PAGE INTENTIONALLY LEFT BLANK

Acknowledgments

For my wife, Haruka, and son, Wyatt, thank you for your support and encouragement along the way to this milestone. Without the two of you allowing me to see the big picture and what this hard task is truly for, I would still be lost on the first page.

For Professor Weatherford, I can't thank you enough for your inspiring and thoughtful stories, knowledge, and guidance to allow me as a student to grow and learn something new and exciting in this career field.

For Travis, thank you for allowing me the opportunity to test these devices and for being the second sounding board for this research. To put it simply, without you I would have no devices to test, and we would never have crossed paths.

For Matt, thank you for taking many days and nights, both fun and challenging, to help me in every aspect of my research and testing to make sure I had the right guidance for this project.

A special thanks to the Defense Threat Reduction Agency for funding this project.

Finally, without the help and support of Ashton Miller, John Mobley, and Levi Owen, I would not have had the proper help and equipment to succeed.

THIS PAGE INTENTIONALLY LEFT BLANK

CHAPTER 1:
Introduction

Gallium Nitride (GaN) based devices have been praised in electronics for their unique properties and versatility in the market. GaN combines the high breakdown field of Silicon Carbide (SiC) with the high frequency characteristics of Gallium Arsenide (GaAs), Indium Phosphide, or Silicon Germanium to give this semiconductor material much more power and advantage than its other group III-V competitors [1].

With the advantages shown in GaN, the military services and other Department of Defense (DoD) organizations have taken interest in its potential applications. GaN semiconductors may provide increased capabilities in every physical domain, including sea, land, air, and space. These devices have high frequency characteristics that make them ideal for radio frequency amplifiers on ships and ground units, and the added benefit of a wide bandgap enables there use on larger buses at higher power levels [2]. Because the space environment is harsh, and because it is extremely costly to launch systems into space, it is important to test the reliability and radiation-hardness of GaN against conditions that the space environment presents.

1.1 Research Objective

GaN ZrO_2 Metal Oxide Semiconductor (MOS) Capacitors provided by U.S. Naval Research Laboratory (NRL) were subjected to radiation damage in order to gain an understanding of defects and damage that might present themselves both in the GaN substrate and ZrO_2 dielectric layer. Devices were characterized to create a baseline for radiation effects testing. Radiation effects testing was done at the Texas A&M University Cyclotron Institute with the K150 cyclotron with a 40 MeV proton beam and 15 MeV argon heavy ion beam. The devices were then re-characterized and the results were compared to the initial testing results. Testing concluded with time-dependent dielectric breakdown (TDDB) tests on select devices. Pre-exposure results were then compared against post-exposure results to determine if oxide breakdowns were influenced by exposure to certain radiation effects.

1.2 Related Work

The majority of research work related to GaN device hardness and reliability involves comparing different gate dielectrics on the substrate to maximize mobility and capacitance in GaN Semiconductor Devices [3].

ZrO_2 and HfO_2 are the latest oxides to be used with GaN MOS Capacitors. Early research comparing these two dielectrics shows promising features for both, as they are high-k dielectrics with improved mobility characteristics. Between the two, ZrO_2 has shown superior results in trap concentration reduction found in the oxide layer. These dielectrics also have the potential to be used for high-frequency applications [3].

Research relating to radiation effects are limited to other GaN devices or MOS capacitors with similar dielectric layers such as HfO_2. In one study, results showed that HfO_2 can be applied to space applications because of its good irradiation resistance [4]. Other research on MOS capacitors include SiO_2 as the dielectric layer and subjected the devices to proton radiation effects. A numerical model of a MOS capacitor was developed to investigate the effects of ionizing radiation and evaluate its post-irradiated condition [5].

Research conducted within the Naval Postgraduate School (NPS) has focused on GaN high electron mobility transistors (HEMTs) and the study of radiation effects with these devices. Wade observed the damage of GaN HEMTs from proton radiation and observed that damage not previously present had occurred under the gates in the device [6]. Research has also been done in conjunction with NRL designed devices. Augustine recently developed SILVACO models on GaN HEMTs based on data and devices designed at NRL and from previous NPS work [7].

1.3 Thesis Organization

This thesis is laid out in the following order. The basics of structure and device properties are covered in Chapter 2 as well as an introduction of radiation effects to electronic devices. Chapter 3 encompasses the entirety of testing and experimentation on the devices. The first section of the chapter goes over device characterization prior to radiation testing. This is followed by the overview of radiation effects testing conducted at the Texas A&M University Cyclotron Institute. The final portion includes post-irradiation testing characterization and

time dependent dielectric breakdown testing. All testing described in this chapter was done utilizing LabVIEW programs and the Agilent B1500A Semiconductor Device Parameter Analyzer. Chapter 4 covers results from each set of testing covered in Chapter 3 and provides comparisons of results from each level. Conclusion and future opportunities for further studies and research are covered in Chapter 5.

THIS PAGE INTENTIONALLY LEFT BLANK

CHAPTER 2:
Background

2.1 Fundamentals of MOS Capacitors

The MOS capacitor is a very important part in some integrated circuits because its ability to store charge allows it to be used as a building block for charged coupled devices. The MOS Capacitor consists of three layers, as shown in Figure 2.1. The top plate of the capacitor is made of metal, the bottom plate of the capacitor is made from p-doped silicon, and the dielectric is made from an oxide of thickness n. An ohmic contact is used to electrically connect to the p-doped silicon [8].

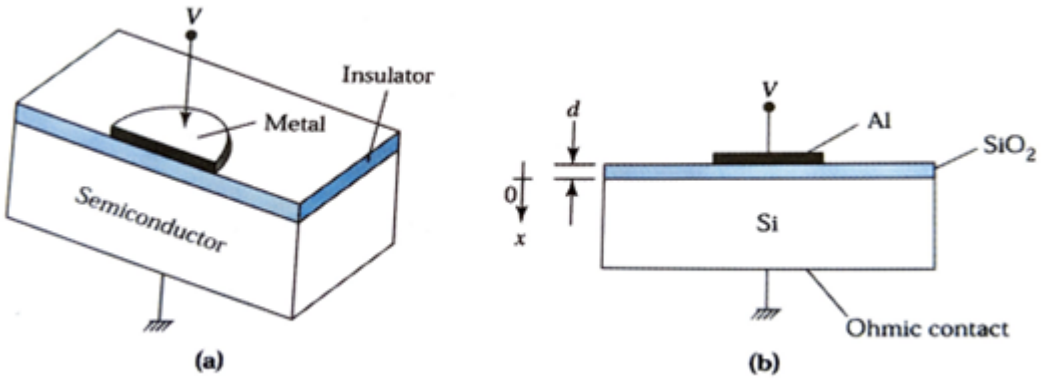

Figure 2.1. Perspective and cross-section view of a MOS capacitor. Source: [8].

The capacitance for a MOS capacitor can be calculated by the following equation:

$$C = \frac{A\epsilon}{d}, \tag{2.1}$$

where ϵ is the permittivity of the insulator, d is the distance between the two plates, and A is the unit area of the structure [9].

The flat-band condition in a MOS capacitor occurs when the metal and semiconductor work-functions are equal, no charges exist in the oxide, and no conduction current (DC) occurs through the oxide [8]. This can be expressed using equation 2.2:

$$q\phi_{ms} = (q\phi_m - q\phi_s) = q\phi_m - (q\chi + \frac{E_g}{2} + q\psi_B) = 0, \tag{2.2}$$

where $q\chi$ is the electron affinity, E_g is the bandgap energy of the semiconductor, and $q\psi_B$ is the difference in energy between the fermi level and intrinsic fermi level. If positive charges accumulate in the oxide, the C-V curve will shift to the left as shown in Figure 2.2a. This shift is more pronounced when the positive charges near the oxide semiconductor interface. Figure 2.2c shows positive charge accumulated and Figure 2.2d shows the negative bias required for flat-band condition [10].

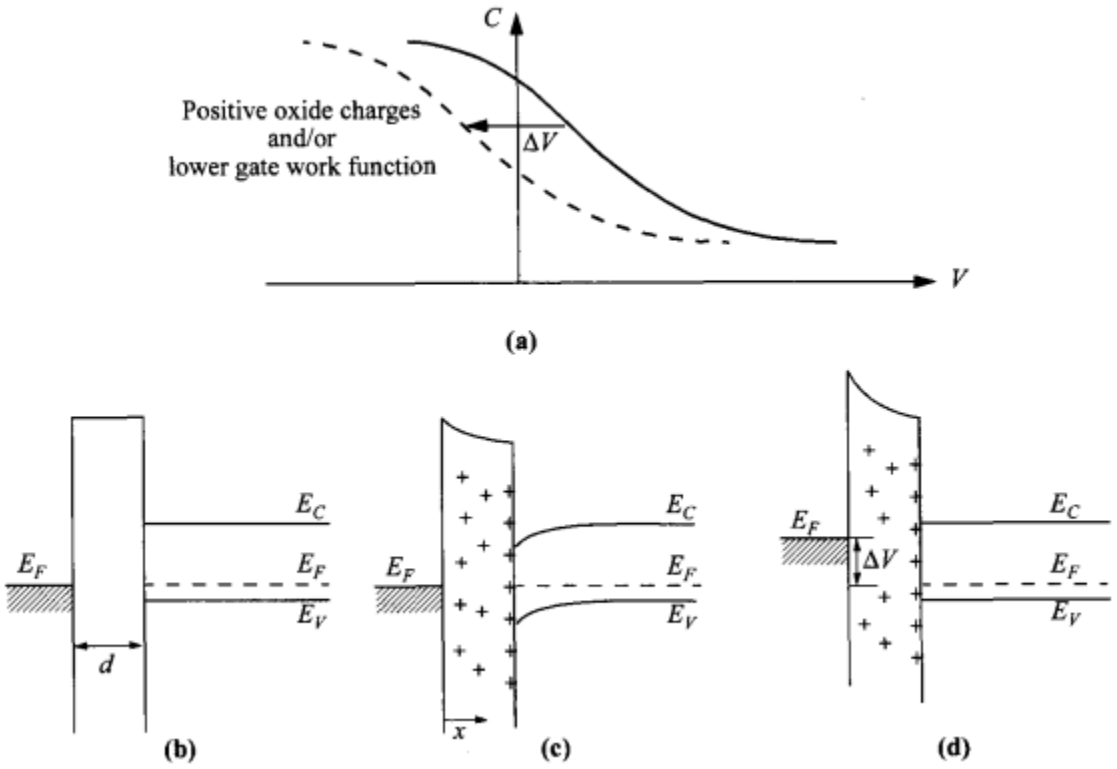

Figure 2.2. (a) High-frequency C-V curve (on p-semiconductor), shifted along the voltage axis due to positive oxide charges; (b) Band diagram at flat band, original; (c) With positive oxide charges; and (d) new flat-band bias. Source: [10].

2.2 Properties of GaN MOS Capacitors

For a large portion of the history of semiconductors, Silicon has dominated the industry. Since the 1990s, universities and industry have made significant advancements in GaN technology, including the development of different color LEDs. GaN semiconductors have been steadily rising in popularity for military applications because of their ability to handle high power at high frequencies [1]. This is especially so in the case for advanced integrated circuit devices to be used in space or other high radiation environments where these devices could provide more efficient and powerful electronics with more reliability [2]. One advancement has been moving from the widely used Si and SiC microelectronics to GaN and GaN/oxide combinations. One GaN oxide combination of recent significance has been

using ZrO_2 as the oxide layer in a MOS Capacitor. GaN is a group III-V semiconductor material notably used for high frequency and high power electronics. GaN properties include a high saturation velocity of $3x10^{17}$ cm/s, high critical electric field of 4.2 MV/cm, and a large band gap of 3.4 eV [11]. The use of this semiconductor improves breakdown voltages and the efficiency of switching transistors.

ZrO_2 is one possible high-k dielectric that can be used on GaN. ZrO_2 has a permittivity of 25 and a band gap of 5.6 eV [12]. High-k dielectrics provide increased gain in a Metal Oxide Semiconductor Field Effect Transistor (MOSFET). G. Zhang et al. mentioned "ZrO_2 has a reasonably high conductance band offset when aligned to GaN. ZrO_2 also has temperature stability and low permeation rates of ambient gases for potentially improving device reliability" [12]. One such study concluded that ZrO_2 displayed high capacitance densities of $7.2\mu F/cm^2$, high mobility of $210cm^2/Vs$, and that samples showed low gate oxide leakage with little dependence on temperature [11].

GaN has shown to be able to outperform in the Figure 2.4 where comparisons of theoretical figure of merit limitations over breakdown voltages show GaN ahead of its silicon competitors by being closer to the optimal application area [13].

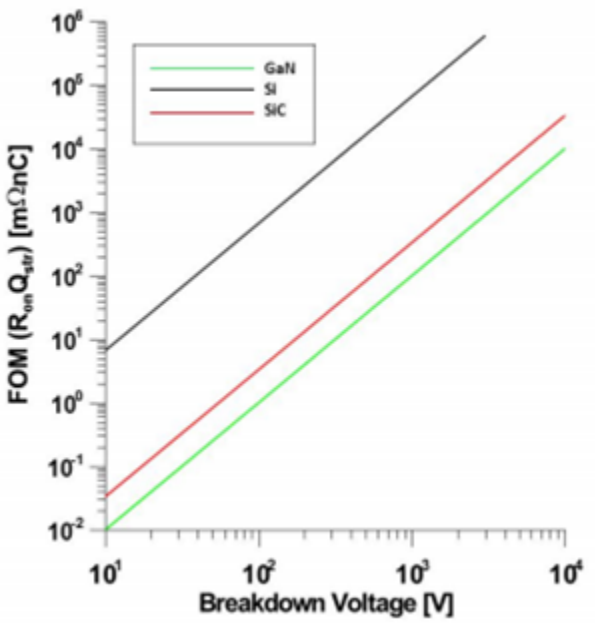

Figure 2.3. Shown is the comparision of the theoretical limiting Figure of Merit of PMAD technology vs. breakdown voltage. Source: [13].

2.3 Radiation Effects

Radiation can cause certain effects to electronics and systems in space. Long-term exposure from the Van Allen Belt, Solar Proton Events, and Galactic Cosmic Rays all cause different effects to systems. Long-term exposure to proton fluxes can induce changes in semiconductor properties. Another serious problem could be the accumulation of charge on insulating material, which can lead to electric field breakdown or shifts in fermi levels. Solar Proton Events are caused by major eruptions on the solar surface of intense high-energy protons and trapped protons in the Van Allen Belts. This can cause larger than normal fluxes, and energies can potentially cause major issues for equipment.

To study displacement and ionization traps in MOS devices, the work investigated proton and heavy ion radiation. We will concentrate on charged particles to include protons and heavy ions. These particles can ionize electrons or cause displacement of lattice atoms. Ionizing radiation is also referred to as total dose effects [14]. These total dose effects or displacement damage can be initiated by Galactic Cosmic Rays, Solar Flares, and interaction with Van

Allen Radiation Belt particles. Charges can accumulate in the oxide or semiconductor layer of MOS devices induced by displacement damage or ionization of electrons or holes can be trapped in defect states [15].

CHAPTER 3:
Experiment

3.1 Composition of Devices and Testing Layout

The GaN ZrO_2 MOS Capacitors used in this study were grown by the Naval Research Laboratory (NRL). These devices were made by depositing the ZrO_2 dielectric layer by Atomic Layer Deposition (ALD). The cross-section of the device is shown in Figure 3.1. The top layer consists of a nickel/gold plate. The dielectric oxide layer is a 40 nm thick layer of ZrO_2 deposited via ALD using zirconium tert-butoxide and tetrakis(dimethylamino)zirconium precursors [16]. The substrate layer is made up of a 2 μm N+ GaN, 250μm N+ GaN, a GaN ohmic layer, and a titanium/gold overlay on the bottom. All biasing and characterization testing was applied using the top nickel/gold plate.

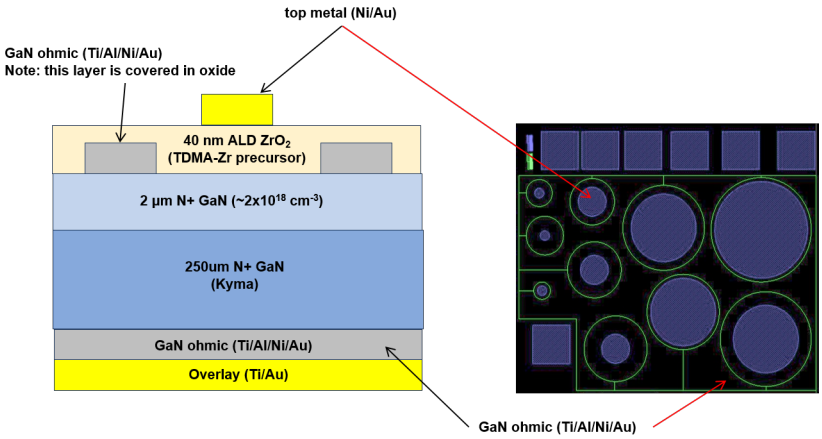

Figure 3.1. Cross-section of GaN MOSCAPs used for radiation exposure testing.

Devices were fabricated in an area of two to four reticles with corresponding numerical identifiers imprinted on each die. Each reticle contained approximately 80 devices that could be connected and tested. Each reticle was then appropriately diced and placed in a QP-QFN7X7-48-500 package. Due to space constraints within the package, only 36 bonds were made to each reticle per package. This work required a Printed Circuit Board (PCB) to

be designed in EAGLE as shown in Figure 3.2 [17]. The test board was interconnected with the Agilent B1500A and a Keithley Switch Matrix. Additionally, a Temperature Controller was fitted underneath the PCB to allow the device to be temperature controlled. A total of 25 reticles with approximately 36 MOS capacitors were bonded and packaged.

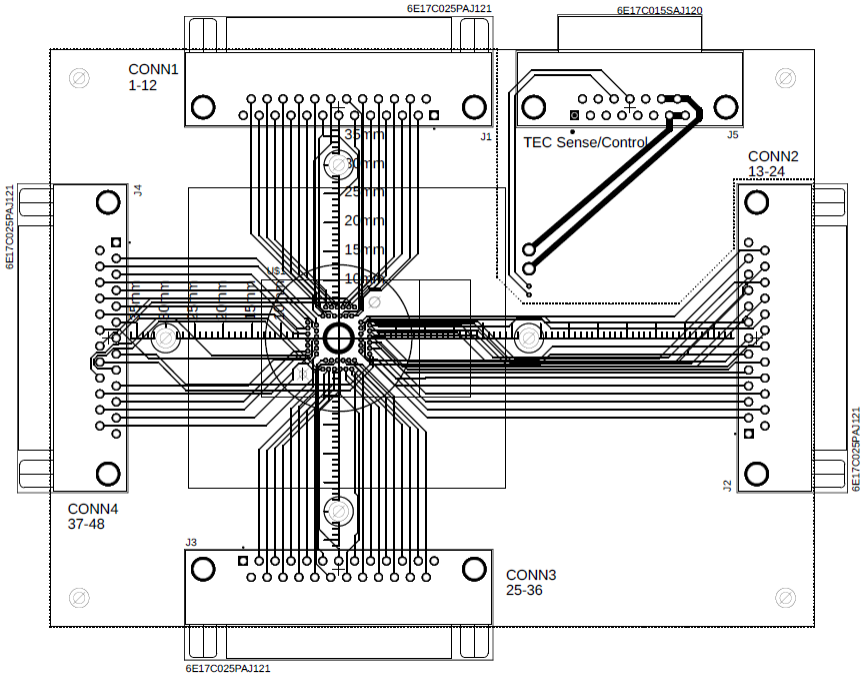

Figure 3.2. Top view of PCB utilized for this work.

Additional drawings and outlines are found in Appendix, Section A1.

3.2 Initial Characterization of Devices

Testing and characterization were done using the custom designed PCB, Agilent B1500A, and a Keithley Switch Matrix. The PCB was connected to the B1500A and switch matrix using DB25 connectors, and the test plan was implemented using LabVIEW for control. A total of 25 reticles were characterized for further testing. Initial characterization of the devices was used to form a data baseline of the devices to be irradiated in the effects testing portion of the research.

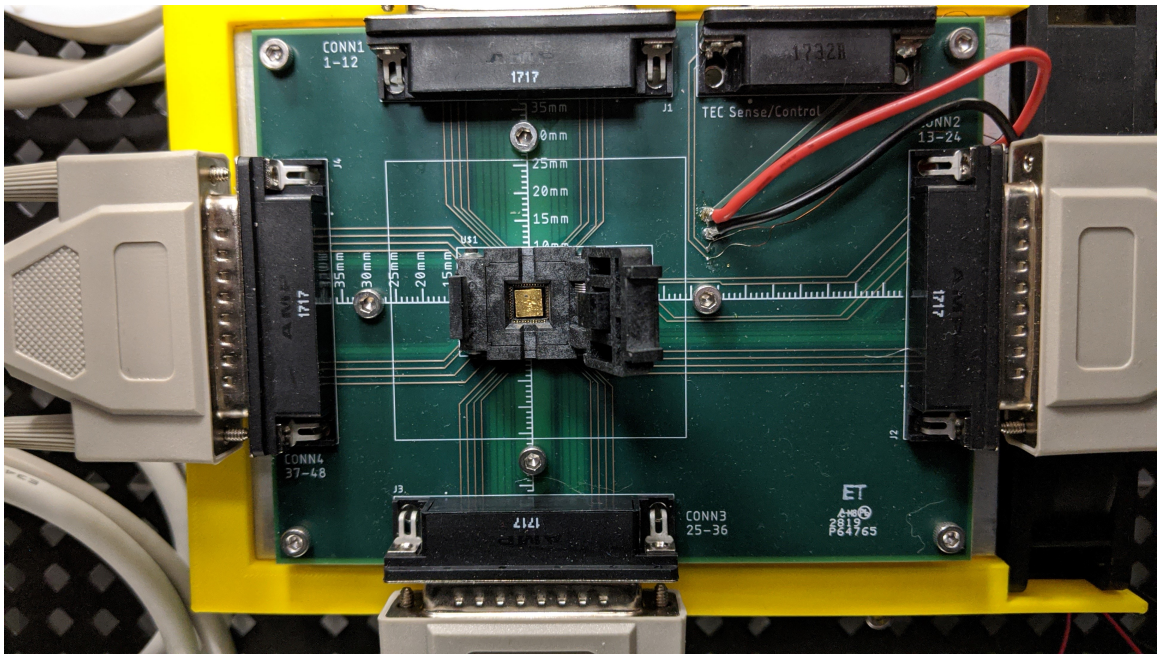

Figure 3.3. PCB used to characterize devices in actual test bed with printed holder.

Each device characterization included a series of Capacitance-Frequency (C-F) tests, Capacitance-Voltage tests (C-V), and Current-Voltage tests (I-V). Table 3.1 shows that each test was set up with different measurements taken for data collection.

Capacitance-Frequency Measurement				
	Sweep mode	Bias Voltage	Start Frequency	Stop Frequency
Measurement 1	Single	0 Vdc	1 kHz	500 kHz
Measurement 2	Single	2 Vdc	1 kHz	500 kHz
Measurement 3	Single	-2 Vdc	1 kHz	500 kHz
Capacitance-Voltage Measurement				
	Sweep mode	Frequency	Start Voltage	Stop Voltage
Measurement 1	Double	500kHz	-6 V	6 V
Measurement 2	Double	500kHz	-7 V	7 V
Measurement 3	Double	500kHz	-8 V	8 V
Measurement 4	Double	500kHz	-9 V	9 V
Measurement 5	Double	500kHz	-10 V	10 V
Current-Voltage Measurement				
	Sweep mode	Current Compliance	Start Voltage	Stop Voltage
Measurement 1	Double	3 mA	-8 V	8 V

Table 3.1. Tables showing each measurement used during characterization.

3.3 Radiation Effects Testing

Radiation effects testing was conducted at the Texas A&M University Cyclotron Institute using the K150 cyclotron. Effects testing was split into three categories: proton dose testing, proton with positive bias testing, and heavy ion with positive bias testing. All proton testing used a 40 MeV beam, and heavy ion testing used a 15 MeV Argon beam. Five reticles were used for dose testing. Four reticles with 12 devices each were selected for proton with positive bias testing. 10 reticles with 12 devices each were selected for heavy ion with positive bias testing.

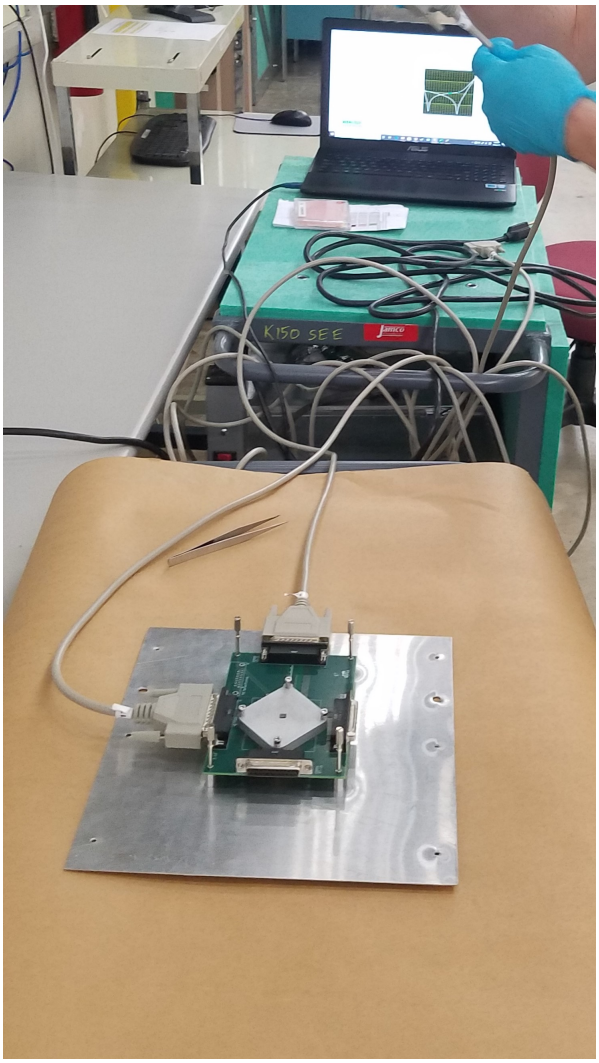

Figure 3.4. Test board used for bias testing at Cyclotron Institute at Texas A&M.

Proton dose exposure was done by placing the five reticles on the in-air station and shorting them to the test board. Dosimetry for exposure started at a flux of $1x10^7 particles/cm^2$ and allowed the beam to get to a nominal fluence of $1x10^8 particles/cm^2$. After each fluence was achieved, one reticle was removed, and the flux was increased by a factor of 10. Each reticle was then subjected to a fluence increase by a factor of 10 until the last reticle was subjected to a fluence of $1x10^{12} particles/cm^2$.

Proton with positive bias testing used the Agilent B1500A and switch matrix to apply a biased voltage during a radiation exposure of 50 seconds at a flux of $1x10^8 particles/cm^2$ or $1x10^9 particles/cm^2$. After each biasing time, all devices were characterized with a C-V test to monitor any changes. Devices were exposed over three different bias voltages of $10.8V, 11V, and 11.2V$ over a total exposure time of 1280 seconds.

Heavy ion testing also used the Agilent B1500A and switch matrix to apply the same bias voltages at the same exposure times as the proton bias testing with an argon heavy ion beam flux of $1x10^8 particles/cm^2$. Total exposure times for the heavy ion beam was limited to 400 seconds.

3.4 Post-Irradiation Characterization and Testing

Post-irradiation characterization utilized the same LabVIEW programs used in Section 1 to analyze the effects on the devices after they were subjected to proton and heavy ion radiation. Retesting encompassed all four proton-dosed reticles, three reticles from proton-biased testing, and 10 of the reticles used for heavy ion-biased testing.

3.5 Time-Dependent Dielectric Breakdown Testing

For analysis of TDDB testing, two reticles from each section of radiation effects testing was selected. A Stress-Measure-Stress LabVIEW program was based on a strategy developed by Warnock and Alamo in which the device underwent a series of C-V measurements that was used to both apply stress and to measure when the stress had stopped [18]. The LabVIEW program stressed all devices at three different positive bias voltages of 10.8V, 11V, and 11.2V for 50 seconds followed by a C-V test taken to determine at what time interval the dielectric broke down. The results were then compared to reticles not irradiated to study whether effects of radiation on the dielectric will affect overall life cycle due to trapped charges or displacement damage in the oxide.

CHAPTER 4:
Results of Analysis

4.1 Analysis of Devices Radiated by Protons

Proton radiation exposure was accomplished with the devices shorted to the back plate of the test platform. Thus, no electric field was applied to the device. Comparing devices pre- and post-radiation, it was observed that exposure to proton radiation decreased the capacitance of the devices tested. Figures 4.1 and 4.2 show C-V measurements from two reticles exposed during proton radiation. It was observed that the devices decreased in capacitance between $40 - 70pF$. Integrating the area of the hysteresis window is associated with an equivalent charge in the device. This charge could be a combination of trapped electrons or holes, or defects acting as donors or acceptors. Comparison between pre- and post-radiation hysteresis showed a decrease of charge by an average of 5%.

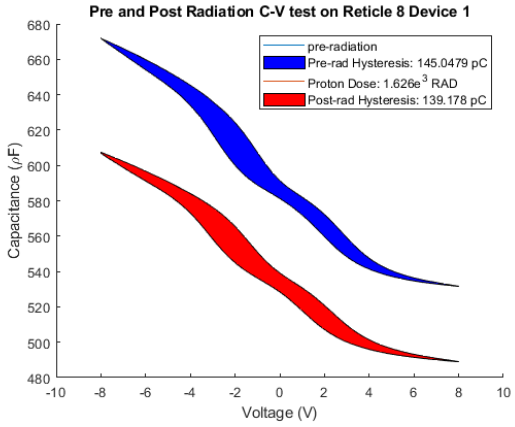

(a)

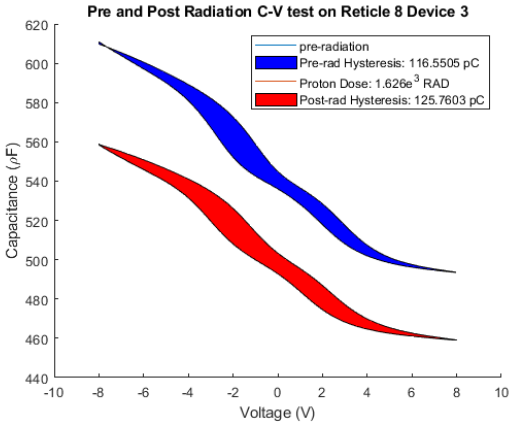

(b)

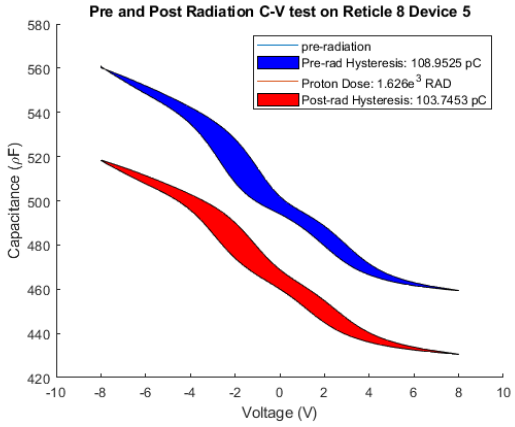

(c)

Figure 4.1. a) - c) shows reticle 8 devices pre- and post-proton dose with short radiation C-V measurements with area of hysteresis.

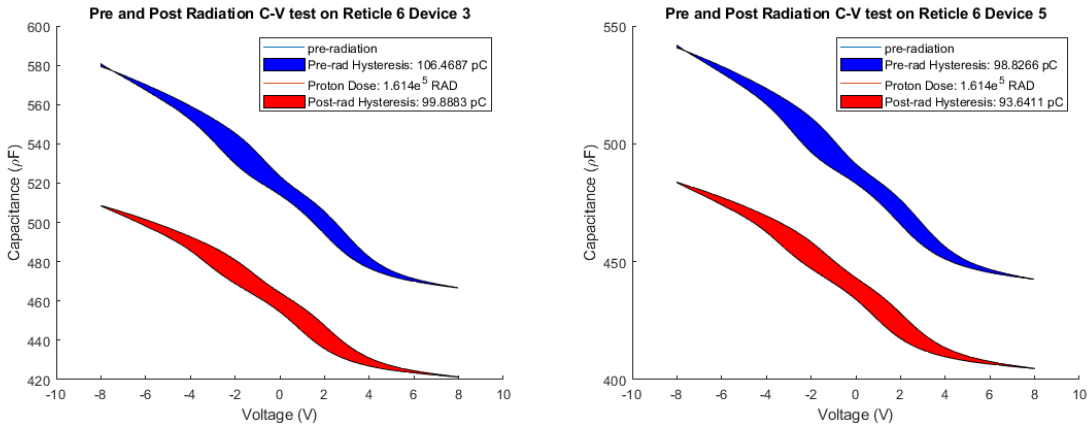

(a) (b)

Figure 4.2. a) and b) shows reticle 6 devices pre- and post-proton dose with short radiation C-V measurements with area of hysteresis.

4.2 Analysis of Parts Radiated by Protons with Positive Bias Voltage

Radiation exposure occurred while devices had three different applied positive bias voltages of $10.8V$, $11V$, and $11.2V$. Pre- and post-radiation with comparisons are as shown in Figure 4.4 showing that while a shift in capacitance did occur, the shift increased the capacitance of the devices between $25 - 30pF$. The comparison of the hysteresis pre- and post-radiation of the C-V measurement increased charge by as much as 20%.

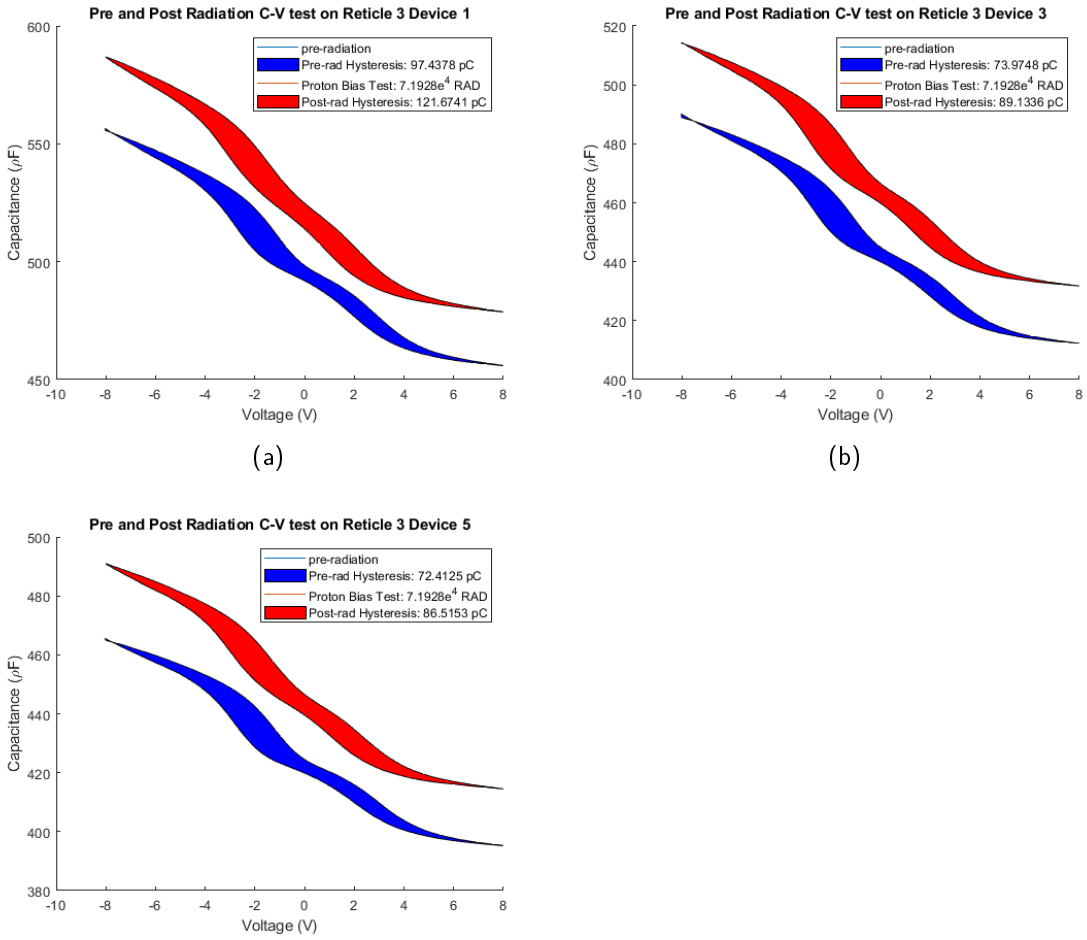

Figure 4.3. a) - c) shows reticle 3 devices pre- and post-proton with positive bias radiation C-V measurements with area of hysteresis.

4.3 Analysis of Parts Radiated by Argon Heavy Ions with Positive Bias Voltage

Heavy ion radiation exposure was also accomplished using the same bias voltage as the proton with bias voltage exposure. Analysis of the C-V measurements are shown in Figures 4.4 and 4.5 for pre and post radiation exposure and show similar results from the proton dose radiation. The decrease in capacitance was smaller in the range of $5 - 25pF$. One device measured a maximum shift of $70pF$. Comparing the pre- and post-radiation hysteresis of

the C-V measurements showed an increase of charge in the area by an average of 8%.

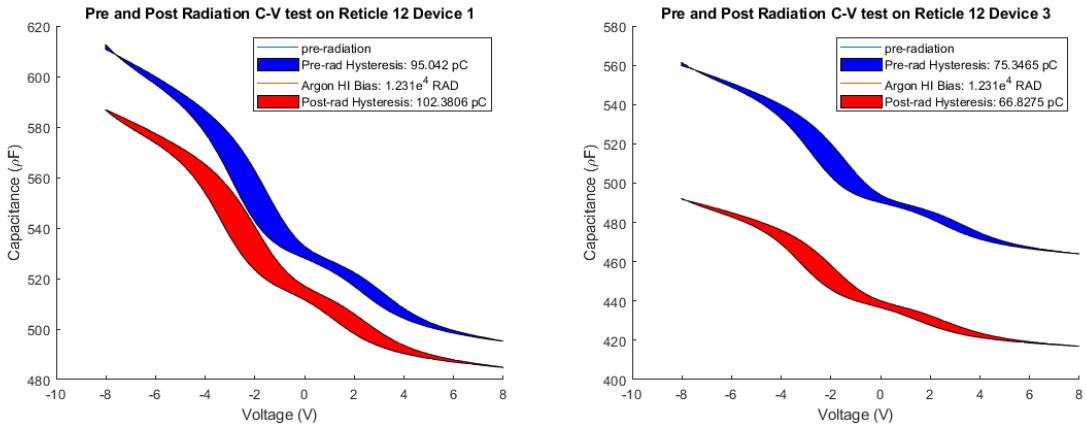

(a) (b)

Figure 4.4. a) and b) shows reticle 12 devices pre- and post-heavy ion with positive bias radiation C-V measurements with area of hysteresis.

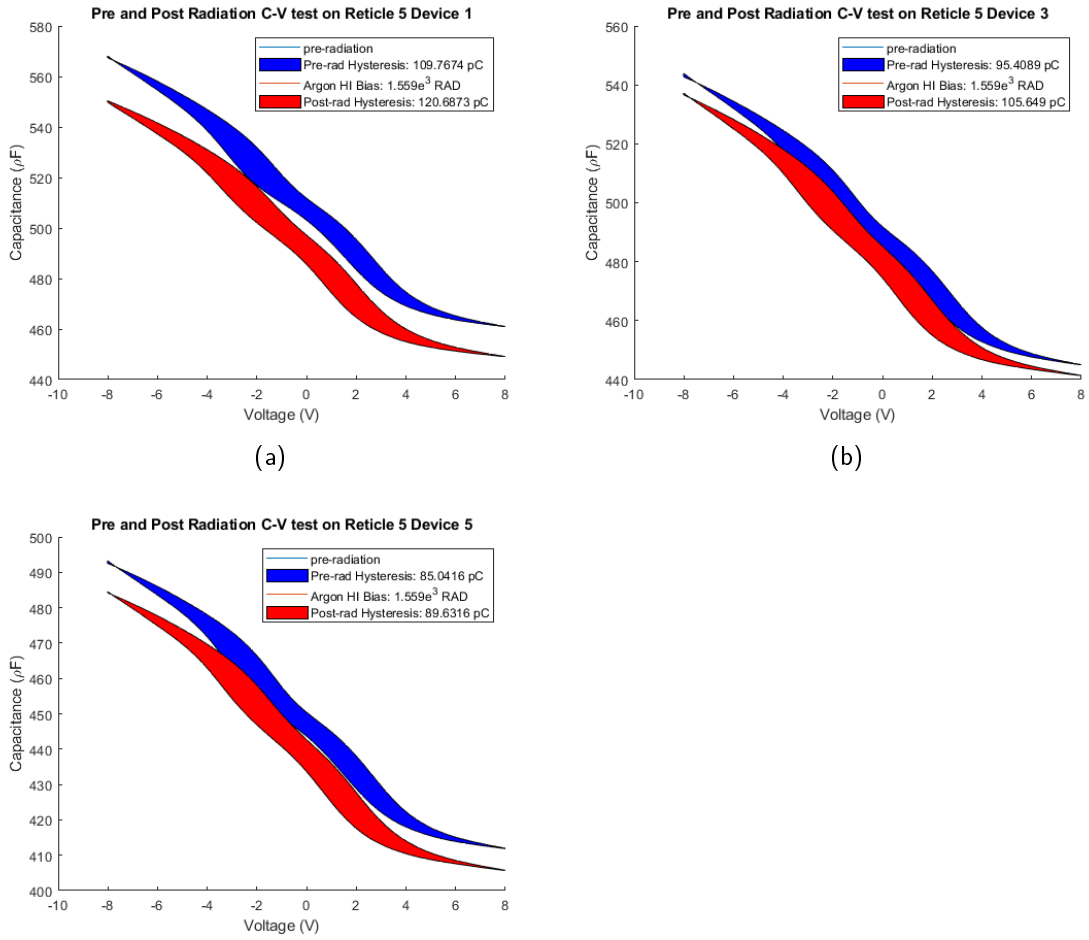

Figure 4.5. a) - c) shows reticle 5 devices pre- and post-heavy ion with positive bias radiation C-V measurements with area of hysteresis.

4.4 Analysis of Time-Dependent Dielectric Breakdown Testing

Preliminary data from time-dependent dielectric breakdown (TDDB) testing shows that the devices exposed to radiation did not have oxide breakdown happen sooner than devices without radiation. There were no major differences between the devices tested in proton and heavy ion beams and their breakdown times. Figure 4.6 shows the scatter plot for the reticles tested by averaging their times and grouped by exposure type. Devices exposed to

radiation showed larger times before oxide breakdown occurred at higher stress voltages. Lower stress voltages showed no difference between no radiation exposure and any type of radiation exposure. Lower voltages also showed earlier breakdown across all exposure types. The longest time before breakdown occurred after exposure to heavy ion radiation was 1250 seconds at a bias of 11.2V. The longest time before breakdown occurred after exposure to proton radiation was 850 seconds at a bias of 11V.

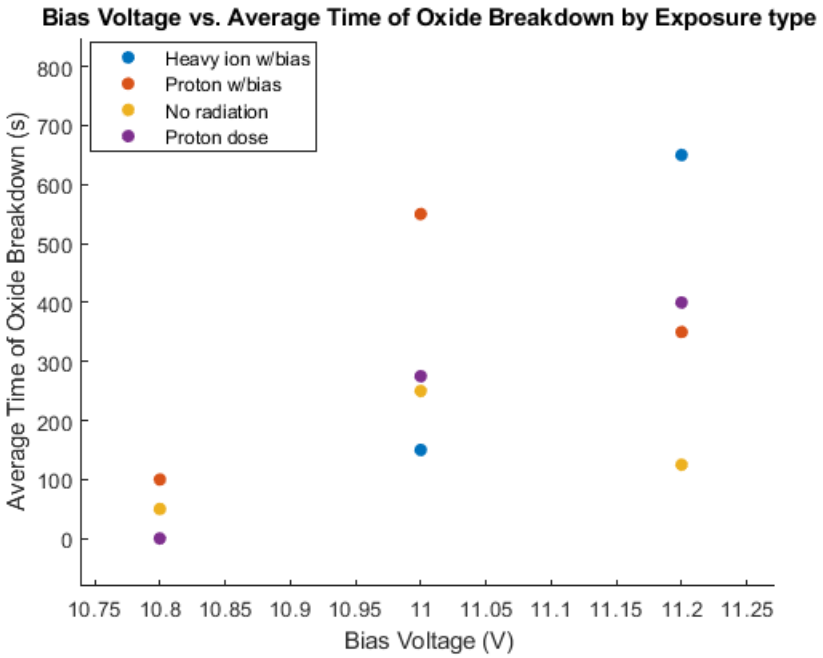

Figure 4.6. Scatter plot showing each exposure type and their average time of oxide breakdown vs. stress voltage

4.5 Discussion of Results

All results of radiation exposure exhibited a shift in their capacitance and a change in the equivalent charge of the device shown by the area of the hysteresis. This could be caused by damage due to high energy particles or ionized charges trapped within the oxide layer. Figure 4.7 illustrates the three cases where Figure 4.7a is shorted to the backplate for proton radiation, Figure 4.7b is heavy ion irradiation with positive stress bias, and Figure 4.7c is proton radiation with positive stress bias. Figure 4.7a has the lowest field in the oxide to separate charges. Figure 4.7b illustrates as ionized charges are trapped inside the oxide

layer from heavy ion radiation, the positive charges could move to the right to the oxide-semiconductor interface. This could also cause a layer of negative charges to be trapped within the oxide layer, adding a series capacitance within the oxide. This collection of trapped charges could be the cause for the decrease in capacitance after exposure to heavy ion radiation. Figure 4.7c shows that due to the proton beam having higher total non-ionizing energy loss (NIEL) than the heavy ion radiation, this could be the cause for negative charge defects within the oxide layer increasing the capacitance after exposure.

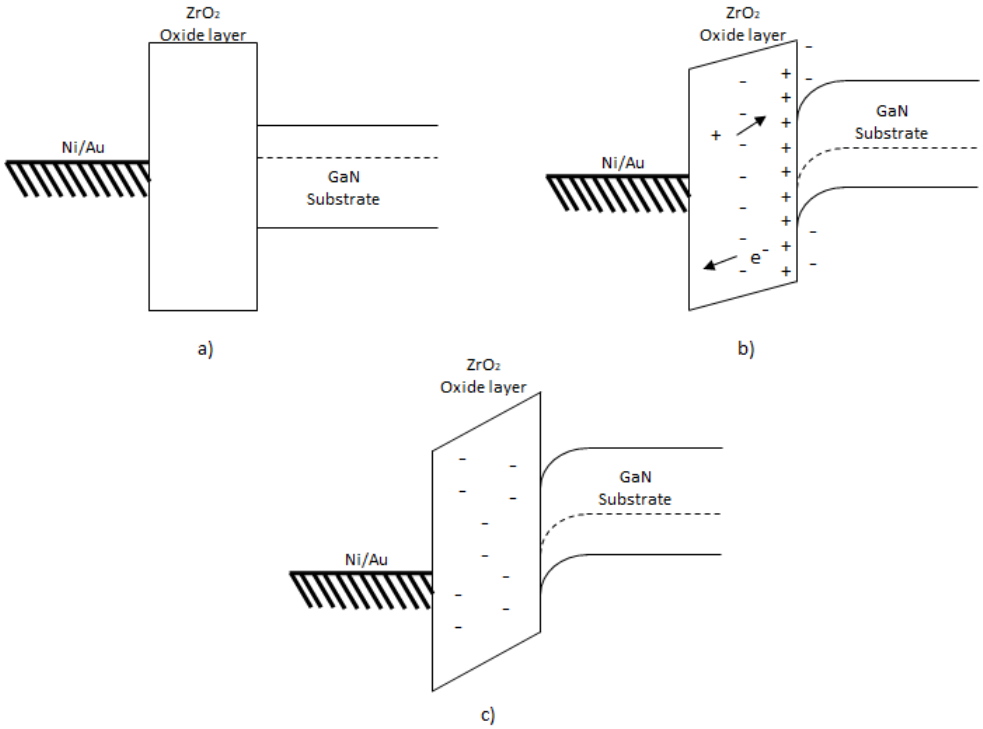

Figure 4.7. a) shows an example of the band diagram of the devices tested at zero bias. Figure b) shows what the band diagram of the devices at bias after heavy ion with positive stress bias radiation exposure. Figure c) shows what the band diagram of the devices after proton with positive stress bias radiation exposure.

Higher stress voltages after exposure had improved oxide breakdown. The positive biases applied during radiation exposure were the same as the stress voltages applied during TDDB measurements, which could trap more positive charges in the oxide. This buildup of holes during exposure could have been the reason for increased time before breakdown as they

could have provided a lower electric field and reduced the capacitance when the stress voltage was applied.

THIS PAGE INTENTIONALLY LEFT BLANK

CHAPTER 5:
Conclusions

Through this research we successfully gained an understanding of radiation effects on GaN ZrO_2 MOS capacitors.

All devices showed a shift in overall capacitance post-radiation exposure, as shown in Chapter 4 using C-V measurements. These results varied depending on the effective fluence on the device and whether the device had a positive bias during exposure. This change of area for the hysteresis may be due to trapped charges from ionization. The two cases, proton irradiated with zero bias and heavy ion irradiated with positive bias could be explained by this ionization effect. Devices that underwent proton beam irradiation with positive bias showed the opposite result with an increase in capacitance. This effect is more likely caused by displacement damage. The higher proton fluence provides more NIEL creating negatively charged defects within the oxide.

TDDB measurements exhibited different behavior than expected. Instead of showing a decrease in oxide breakdown time, certain irradiated devices showed an increased survival at high stress of the device, with some lasting two to four times longer than devices with no exposure. TDDB measurements also showed more sensitivity to lower bias voltages than higher bias voltages. It appears that this data has no correlation with TDDB under stress bias.

This avenue of research is proving paramount to the DoD and partners as radiation-hard devices are being integrated into more high power and high frequency systems that require more reliability in space and radiation environments. Topics and research that expand this study allow these devices to be implemented in more applications today.

5.1 Future Work Considerations

Because these devices were created solely for this research work, recommendations for future work are limited. Due to testing limitations, the thermal electric cooler was not used for characterization and TDDB testing. Not all devices were subjected to radiation

effects and TDDB testing. With the addition of a temperature controller in the test board, characterization and TDDB can be analyzed and compared with different temperature settings to the data gained from this research. Research could also be conducted to design and implement a model in SILVACO. This physically-based simulation software allows users to create 2D and 3D models of semiconductor devices [19]. Research on the model could be used to determine expected effects for higher fluences and identifying trap levels for targeted radiation exposure at different energy levels.

APPENDIX: Additional Figure and Tables

A.1 Test Layout for QFN chip

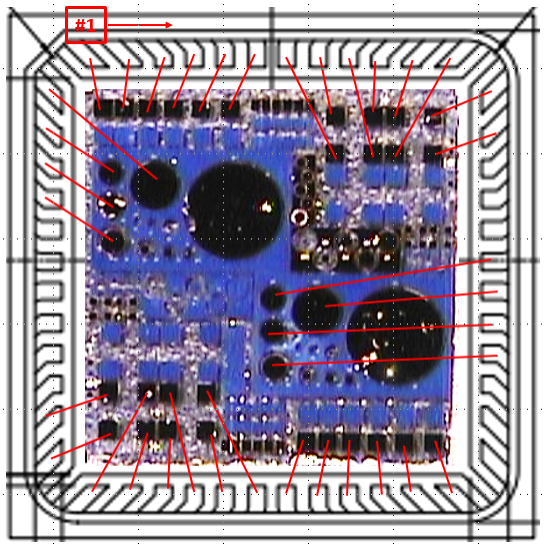

Figure A.1. Bonding diagram of reticles in QFN packaging

A.2 Radiation Test Plan

ZrO2 Gan MOSCAPS Dose

BEAM	device id	flux (ions/cm^2)	avg flux (ions/cm^2)	fluence (ions/cm^2)	effective fluence (ions/cm^2)	dose (rads)	time (min:sec)
39.5 MeV/u	**RET15**	1.00E+06	1.62E+06	1.00E+08	9.96E+07	1.61E+01	1:14
39.5 MeV/u	**RET7**	1.00E+07	1.35E+07	1.00E+09	9.95E+08	1.61E+02	1:22
39.5 MeV/u	**RET8**	1.00E+08	1.88E+08	1.00E+10	1.01E+10	1.63E+03	1:37
39.5 MeV/u	**RET13**	1.00E+09	1.38E+09	1.00E+11	1.00E+11	1.62E+04	1:20
39.5 MeV/u	**RET6**	1.00E+09	1.24E+09	1.00E+12	1.00E+12	1.61E+05	13:27

Table A.1. Table showing each device tested during dose radiation with device shorted for 40MeV proton beam.

ZrO2 Gan MOSCAPS Proton Bias										
BEAM	**device id**	**bias1 (10.8V)**	**bias2 (11V)**	**bias3 (11.2V)**	**flux (ions/cm^2)**	**avg flux (ions/cm^2)**	**fluence (ions/cm^2)**	**effective fluence (ions/cm^2)**	**dose (rads)**	**time (min:sec)**
39.5 MeV/u	**RET3**	DEV1,7,25,5	DEV3,9,26,11	DEV4,10,27,32	1.00E+08	1.72E+08	1.32E+11	2.07845E+11	3.35E+04	21:09
39.5 MeV/u	**RET9**	DEV1,8,25,5	DEV2,9,26,13	DEV4,10,27,29	1.00E+09	1.21E+09	1.32E+12	1.50867E+12	2.43E+05	21:10
39.5 MeV/u	**RE14**	DEV1,8,25,5	DEV2,9,26,11	DEV3,10,28,29	1.00E+09	1.07E+09	1.32E+12	1.47722E+12	2.38E+05	21:09

Table A.2. Table showing each device tested during proton with positive bias testing for 40MeV proton beam.

ZrO2 Gan MOSCAPS Heavy Ion Bias										
BEAM	**Device**	**bias1 (10.8V)**	**bias2 (11V)**	**bias3 (11.2V)**	**Ion**	**flux (ions/cm^2)**	**avg flux (ions/cm^2)**	**effective fluence (ions/cm^2)**	**dose (rads)**	**time (min:sec)**
11.6 MeV/u	**RET4**	dev1,8,25,6	dev4,10,26,14	dev5,11,27,28	Ar	1.00E+07	1.25E+07	2.20E+08	5.53E+05	6:38
11.6 MeV/u	**RET5**	dev1,8,26,5	dev2,9,27,11	dev3,10,27,29	Ar	1.00E+07	1.22E+07	2.15E+08	6.86E+07	6:39
11.6 MeV/u	**RET12**	dev1,8,26,5	dev2,9,27,11	dev3,10,28,29	Ar	1.00E+07	1.18E+07	2.20E+08	5.53E+05	6:40
11.6 MeV/u	**RET16**	dev1,8,25,5	dev2,9,27,11	dev3,10,28,29	Ar	1.00E+07	1.20E+07	2.10E+08	5.27E+05	6:40
11.6 MeV/u	**RET17**	dev1,8,25,5	dev2,9,27,11	dev3,10,28,29	Ar	1.00E+07	1.17E+07	2.07E+08	5.20E+05	6:38
11.6 MeV/u	**RET18**	dev1,7,26,5	dev2,8,27,11	dev3,10,28,29	Ar	1.00E+07	1.20E+07	2.18E+08	5.22E+05	6:38
11.6 MeV/u	**RET19**	dev1,8,25,5	dev2,26,9,11	dev3,10,28,29	Ar	1.00E+05	1.31E+07	5.75E+05	1.56E+03	1:36
11.6 MeV/u	**RET20**	dev1,7,25,5	dev2,26,8,13	dev3,9,28,29	Ar	1.00E+07	1.25E+07	4.20E+07	1.05E+05	1:19
11.6 MeV/u	**RET22**	dev1,7,26,4	dev2,28,8,11	dev3,9,29,30	Ar	1.00E+07	1.27E+07	4.15E+07	1.04E+05	1:20

Table A.3. Table showing each device tested during heavy ion with positive bias testing for 15MeV argon beam.

List of References

[1] L. F. Eastman and U. K. Mishra, "The toughest transistor yet [gan transistors]," *IEEE Spectrum*, vol. 39, no. 5, pp. 28–33, 2002.

[2] R. T. Kemerley, H. B. Wallace, and M. N. Yoder, "Impact of wide bandgap microwave devices on dod systems," *Proceedings of the IEEE*, vol. 90, no. 6, pp. 1059–1064, 2002.

[3] K. M. Bothe, P. A. von Hauff, A. Afshar, A. Foroughi-Abari, K. C. Cadien, and D. W. Barlage, "Electrical comparison of hfo_2 and zro_2 gate dielectrics on gan," *IEEE transactions on electron devices*, vol. 60, no. 12, pp. 4119–4124, 2013.

[4] Y. Xu, J. Bi, G. Xu, K. Xi, B. Li, and M. Liu, "Total ionizing dose effects and annealing behaviors of hfo 2-based mos capacitor," *Science China Information Sciences*, vol. 60, no. 12, p. 120401, 2017.

[5] R. Chauhan and P. Chakrabarti, "Effect of ionizing radiation on mos capacitors," *Microelectronics journal*, vol. 33, no. 3, pp. 197–203, 2002.

[6] M. G. Wade, "Proton irradiation-induced metal voids in gallium nitride high electron mobility transistors," Master's thesis, Dept. of Elec. Eng., NPS, Monterey, CA, USA, 2015. Available: https://calhoun.nps.edu/handle/10945/47342

[7] R. T. Augustine, "Analysis of proton radiation effects on gallium nitride high electron mobility transistors," Master's thesis, Dept. of Elec. Eng., NPS, Monterey, CA, USA, 2017. Available: https://calhoun.nps.edu/handle/10945/52977

[8] S. M. Sze, *Semiconductor Devices: Physics and Technology*. John Wiley & Sons, 2013.

[9] D. Neamen, *Semiconductor physics and devices*. McGraw-Hill Higher Education, 2003.

[10] S. M. Sze and K. K. Ng, *Physics of Semiconductor Devices*. John wiley & sons, 2006.

[11] P. von Hauff, K. Bothe, A. Afshar, A. Foroughii, D. Barlage, and K. Cadien, "High mobility ($210 cm^2/vs$), high capacitance ($7.2 \mu f/cm^2$) zro_2 on gan metal oxide semiconductor capacitor via ald," in *CS MANTEHC Conference, Boston*, 2012.

[12] G. Zhang, M. Zheng, J. Wan, H. Wu, and C. Liu, "Gan metal-oxide-semiconductor devices with zro2 as dielectric layers," *Applied Surface Science*, vol. 469, pp. 98–102, 2019.

[13] L. Scheick, "Gallium nitride–worth the hype?" *JPL/OSMS Assurance Technology Program Office (ATPO), NASA*, vol. 4, no. 2, 2012.

[14] T. E. Weatherford, "class notes for radiation effects in microelectronics," Dept. of Elec. Eng., Naval Postgraduate School, Monterey, CA, USA, spring 2020.

[15] "Why space radiation matters," NASA, 2019, [Online]. Available: https://www.nasa.gov/analogs/nsrl/why-space-radiation-matters

[16] T. J. Anderson, V. D. Wheeler, D. I. Shahin, M. J. Tadjer, A. D. Koehler, K. D. Hobart, A. Christou, F. J. Kub, and C. R. Eddy Jr, "Enhancement mode algan/gan mos high-electron-mobility transistors with zro2 gate dielectric deposited by atomic layer deposition," *Applied Physics Express*, vol. 9, no. 7, p. 071003, 2016.

[17] *EAGLE Manual Version 5*, CadSoft Computer, Pembroke Pines, FL, USA, 2010.

[18] S. Warnock and J. A. del Alamo, "Stress and characterization strategies to assess oxide breakdown in high-voltage gan field-effect transistors," in *Compound Semiconductor Manuf. Technol. Conf*, 2015, pp. 311–314.

[19] D. S. Atlas, *Atlas user's manual*, Silvaco International Software, Santa Clara, CA, USA, 2016.

Initial Distribution List

1. Defense Technical Information Center
   Ft. Belvoir, Virginia

2. Dudley Knox Library
   Naval Postgraduate School
   Monterey, California